Published OnlineFirst September 25, 2015; DOI: 10.1158/2159-8290.CD-15-0892

RESEARCH ARTICLE

Infection Exposure Is a Causal Factor in B-cell Precursor Acute Lymphoblastic Leukemia as a Result of *Pax5*-Inherited Susceptibility

Alberto Martín-Lorenzo[1,2], Julia Hauer[3], Carolina Vicente-Dueñas[1,2], Franziska Auer[3], Inés González-Herrero[1,2], Idoia García-Ramírez[1,2], Sebastian Ginzel[3,4], Ralf Thiele[4], Stefan N. Constantinescu[5], Christoph Bartenhagen[6], Martin Dugas[6], Michael Gombert[3], Daniel Schäfer[3], Oscar Blanco[7], Andrea Mayado[8], Alberto Orfao[8], Diego Alonso-López[9], Javier De Las Rivas[9,10], César Cobaleda[11], Maria Begoña García-Cenador[12], Francisco Javier García-Criado[12], Isidro Sánchez-García[1,2], and Arndt Borkhardt[3]

ABSTRACT Earlier in the past century, infections were regarded as the most likely cause of childhood B-cell precursor acute lymphoblastic leukemia (pB-ALL). However, there is a lack of relevant biologic evidence supporting this hypothesis. We present *in vivo* genetic evidence mechanistically connecting inherited susceptibility to pB-ALL and postnatal infections by showing that pB-ALL was initiated in *Pax5* heterozygous mice only when they were exposed to common pathogens. Strikingly, these murine pB-ALLs closely resemble the human disease. Tumor exome sequencing revealed activating somatic, nonsynonymous mutations of *Jak3* as a second hit. Transplantation experiments and deep sequencing suggest that inactivating mutations in *Pax5* promote leukemogenesis by creating an aberrant progenitor compartment that is susceptible to malignant transformation through accumulation of secondary *Jak3* mutations. Thus, treatment of $Pax5^{+/-}$ leukemic cells with specific JAK1/3 inhibitors resulted in increased apoptosis. These results uncover the causal role of infection in pB-ALL development.

SIGNIFICANCE: These results demonstrate that delayed infection exposure is a causal factor in pB-ALL. Therefore, these findings have critical implications for the understanding of the pathogenesis of leukemia and for the development of novel therapies for this disease. *Cancer Discov; 5(12); 1328–43. ©2015 AACR.*

See related commentary by Greaves and Müschen, p. 1244.

[1]Experimental Therapeutics and Translational Oncology Program, Instituto de Biología Molecular y Celular del Cáncer, CSIC/Universidad de Salamanca, Campus M. de Unamuno s/n, Salamanca, Spain. [2]Institute of Biomedical Research of Salamanca (IBSAL), Salamanca, Spain. [3]Department of Pediatric Oncology, Hematology and Clinical Immunology, Heinrich-Heine University Dusseldorf, Medical Faculty, Dusseldorf, Germany. [4]Department of Computer Science, Bonn-Rhein-Sieg University of Applied Sciences, Sankt Augustin, Germany. [5]Ludwig Institute for Cancer Research Brussels and Université catholique de Louvain, de Duve Institute, Brussels, Belgium. [6]Institute of Medical Informatics, University of Muenster, Muenster, Germany. [7]Departamento de Anatomía Patológica, Universidad de Salamanca, Salamanca, Spain. [8]Servicio de Citometría and Departamento de Medicina, Universidad de Salamanca, Salamanca, Spain. [9]Bioinformatics Unit, Cancer Research Center (CSIC-USAL), Salamanca, Spain. [10]Bioinformatics and Functional Genomics Research Group, Cancer Research Center (CSIC-USAL), Salamanca, Spain. [11]Centro de Biología Molecular Severo Ochoa; CSIC/Universidad Autónoma de Madrid; Campus de Cantoblanco, Madrid, Spain. [12]Departamento de Cirugía, Universidad de Salamanca, Salamanca, Spain.

Note: Supplementary data for this article are available at Cancer Discovery Online (http://cancerdiscovery.aacrjournals.org/).

A. Martín-Lorenzo, J. Hauer, and C. Vicente-Dueñas are co-first authors of this article.

I. Sánchez-García and A. Borkhardt are co-senior authors of this article.

Corresponding Authors: Arndt Borkhardt, Heinrich-Heine University Dusseldorf, Moorenstrasse 5, 40225 Düsseldorf, Germany. Phone: 0049-211-81-17680; Fax: 0049-211-81-16707; E-mail: Arndt.Borkhardt@med.uni-duesseldorf.de; and I. Sánchez-García, Instituto de Biologia Molecular y Celular del Cancer (IBMCC), CSIC/Universidad de Salamanca, Campus M. de Unamuno s/n, 37007 Salamanca, Spain. Phone: 34-923-238403; Fax: 34-923-294813; E-mail: isg@usal.es

doi: 10.1158/2159-8290.CD-15-0892

Published OnlineFirst September 25, 2015; DOI: 10.1158/2159-8290.CD-15-0892

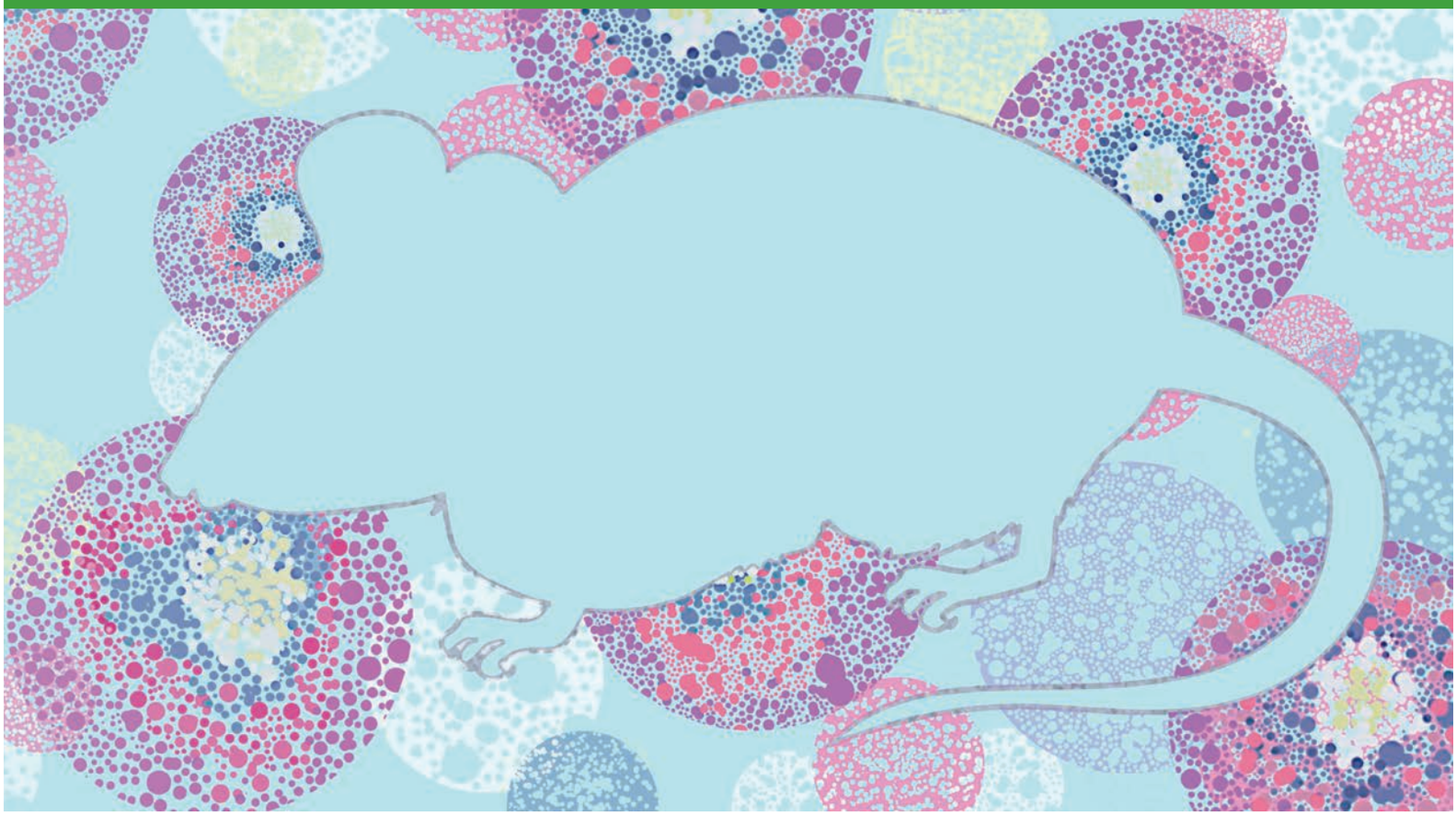

INTRODUCTION

Childhood B-cell precursor acute lymphoblastic leukemia (pB-ALL) is the most common cancer in childhood. The overall cure rate is excellent (approximately 90%); however, treatment is associated with severe toxic side effects and long-term sequelae, and 20% of children still relapse and may later succumb to their disease. Preventional strategies are clearly superior to any therapy improvement. The prerequisite to develop these strategies is to discover the etiology of pB-ALL (1). Somatic alterations of the lymphoid transcription factor gene *PAX5* are a hallmark of pB-ALL (2–4), and recent discoveries of inherited mutations of *PAX5* in a new syndrome of susceptibility to pre–B-cell neoplasia have extended the role of *PAX5* alterations in the pathogenesis of pB-ALL (5, 6). The presence of the inherited mutations of *PAX5* seems to produce a persistent and hidden preleukemic clone that may convert to pB-ALL in only 30% of the family members who carry the mutation (5). Thus, the *PAX5* syndrome shows incomplete penetrance, and the mechanisms responsible for the conversion of the preleukemic clone into full-blown pB-ALL are not known.

Over the past century, infections have been regarded as the most likely cause of childhood leukemia (7). In 1988, two specific hypotheses were proposed that implicated infection as an important causal factor in childhood leukemia: the Kinlen "population-mixing" hypothesis (8) and the "delayed-infection" hypothesis (9). Although the two hypotheses differ in detail and hypothetical mechanism, they do share common ground, as both postulate that childhood leukemia is a consequence of a rare response to common infections (1). These studies suggested that the lack of timely exposure to infections in postnatal life in the clean environments of developed societies might predispose the immune system to aberrant or pathologic responses following subsequent or "delayed" exposure to common pathogens. Descriptive epidemiologic studies support infection as a causal factor in childhood leukemia (10, 11). However, there is no evidence supporting delayed exposure to infection as a second hit related to the natural history of the disease with prenatal initiation (1). Integrating these conflicting data has proven challenging.

In this work, we have explored the role of infections in the development of pB-ALL using a *Pax5* heterozygous model, as recently germline mutations in *PAX5* have been described as conferring an inherited risk to pB-ALL in three kindreds from different ethnic backgrounds (5, 6). We present *in vivo* genetic evidence mechanistically connecting inherited susceptibility to pB-ALL and postnatal infections by showing that pB-ALL was initiated in $Pax5^{+/-}$ mice only when they were exposed to common pathogens. Strikingly, these pB-ALLs closely resemble the human disease in pathology, genomic lesions, and leukemia-associated transcripts. Transplantation experiments and deep sequencing suggest that inactivating mutations in *Pax5* promote leukemogenesis by creating an aberrant progenitor compartment that is susceptible to malignant transformation through the accumulation of secondary *Jak3* mutations. Therefore, this model proves for the

Published OnlineFirst September 25, 2015; DOI: 10.1158/2159-8290.CD-15-0892

first time that delayed exposure to infection triggers pB-ALL development.

RESULTS

Exposure to Common Pathogens Generates pB-ALL in *Pax5*$^{+/-}$ Mice

Recently, germline mutations in *PAX5* have been described as conferring an inherited risk for pB-ALL in three kindreds from different ethnical backgrounds (5, 6). *Pax5* is required for normal B-cell development (12–15), although *Pax5* heterozygous mice do not spontaneously develop pB-ALL (16). Thus, we initially asked if we could provoke pB-ALL development in *Pax5*$^{+/-}$ mice by exposing them to common pathogens. To test this hypothesis, the first group was composed of *Pax5*$^{+/-}$ mice and control littermate wild-type (WT) mice born and kept in a specific pathogen-free (SPF) environment during their lifespan. These *Pax5*$^{+/-}$ mice did not spontaneously develop pB-ALL after 2 years, corroborating previous results (16, 17). The second group was composed of *Pax5*$^{+/-}$ mice and control littermate WT mice born and kept in the SPF environment until moved to a common infectious environment (Fig. 1A). The microbiologic status in the conventional facility was defined and controlled for 2 years (Supplementary Table S1; Supplementary Fig. S1). Under this scenario, specific pB-ALL development was observed in 22% (9 of 41) of *Pax5*$^{+/-}$ animals but not in WT mice (Fig. 1B, C, and D), closely resembling the low penetrance of pB-ALL development in the families with the heterozygous *PAX5* c.547G>A mutation (5, 6). The appearance of leukemia in *Pax5*$^{+/-}$ mice occurred between 6 and 16 months of age. This is independent of a crucial time point of exposure to infection, as pB-ALL appeared in mice that were transferred to a conventional animal facility between 2 and 5 months of age. These pB-ALLs became manifest with splenomegaly, disruption of splenic architecture due to blast infiltration, and appearance of blast cells in the peripheral blood (PB; Fig. 1C). FACS analysis revealed a cell surface phenotype of CD19$^{+/-}$B220^{+}IgM^{-}cKIT$^{+/-}$CD25$^{+/-}$ for tumor cells that extended through bone marrow (BM), PB, spleen, and lymph nodes (Fig. 1D; Supplementary Fig. S2A and S2B) and infiltrated nonlymphoid tissues like liver, kidney, and lung (Supplementary Fig. S2C). All pB-ALLs displayed clonal immature B-cell receptor (BCR) rearrangement (Fig. 1E). To explore the relevance of our findings for human leukemia, we next identified 4,511 significantly repressed and 3,929 significantly induced genes (FDR = 0.005) in tumor-bearing BM from *Pax5*$^{+/-}$ mice compared with BM-derived B220^{+} cells from WT mice (Fig. 2A, left; Supplementary Table S2), including increased expression of genes with roles in progenitor and stem cell compartments of BM and with significant enrichment in human B-ALL gene sets [refs. 18, 19; Gene Set Enrichment Analysis (GSEA) FDR = 0.000; FDR = 0.000] as well as significant alignment with the pro–B-cell stage of differentiation (refs. 20, 21; GSEA up genes FDR = 0.000; down genes FDR = 0.000; Supplementary Fig. S2D). In order to rule out that the heterogeneity of the control B cells could also contribute to the observed differential gene expression, we characterized the global expression signature of purified WT pro/pre-B cells and compared with the expression signature of *Pax5*$^{+/-}$ leukemias. The analysis showed a similar differential gene expression profile (Fig. 2A, right).

The universal finding of deletion of the WT *PAX5* allele and retention of the hypomorphic *PAX5* c.547G>A allele in human pB-ALL suggests that very reduced activity of WT PAX5 is required to establish the leukemic clone (6). Thus, we next investigated the status of *Pax5* in mouse pB-ALL. The majority of the murine *Pax5*$^{+/-}$ pB-ALL (5/9; 55.6%) did not express CD19 (Table 1), suggesting loss or marked reduction of *Pax5* activity, which is in agreement with gene expression analysis of murine *Pax5*$^{+/-}$ tumors showing reduced transcriptional activity of PAX5, similar to what is found in human leukemia (refs. 5, 6; Supplementary Fig. S2E; Supplementary Tables S2 and S3). In this sense, whole-exome sequencing analysis of 8 of 9 *Pax5*$^{+/-}$ pB-ALL identified two cases involving the acquisition of an additional *Pax5* mutation, which were the presence of a *Pax5* variant, p.Pro80Arg (2), causing reduced PAX5 transcriptional activity in humans and a second *Pax5* variant, p.Pro80Leu. However, our finding that 4 murine pB-ALL tumor cells expressed CD19 (Table 1) suggests that a complete loss of PAX5 activity is not required to establish the leukemic clone in a significant percentage of cases. In addition, in 100% of cases these human pB-ALLs displayed homozygous loss of the *CDKN2A* (*p19ARF/INK4A*) tumor suppressor locus (5, 6). In 2 of 5 murine pB-ALLs, *p19Arf* expression was absent (Fig. 2B), correlating in one mouse (O361) with genomic loss of the *Cdkn2a* locus (Fig. 2C). Overall, these results provide evidence that this murine model closely reproduces the human disease phenotype with respect to clinical and molecular/genetic aspects. It represents the first proof that delayed exposure to infection can induce human-like pB-ALL in mice with an inherited genetic predisposition at reduced penetrance.

Exposure to Infection in *Pax5*$^{+/-}$ pB-ALL Development

To identify the types of pathogens in the conventional facility, we monitored the health status of the respective animals. In the SPF facility, animals are pathogen free according to the serological analysis carried out (Supplementary Table S1). When transferred to the conventional animal facility, mice are exposed to a variety of pathogens, among them murine norovirus, mouse hepatitis virus, helicobacter species, and trichomonas muris (Supplementary Fig. S1), inciting a significant immune response in the animals. In order to exclude insertional mutagenesis and leukemia development on the basis of viral integration, we carried out whole-genome sequencing of three *Pax5*$^{+/-}$ pB-ALLs. This experimental approach was very sensitive as it was able to detect a single 127 bp integration into exon 2 of the *Pax5* locus in all three tumor samples and control mice. This is the SV40 nuclear localization signal inserted together with the targeting vector into *Pax5* exon 2 for generation of the *Pax5*$^{-/-}$ mice (15). The sequence serves as positive control to prove this approach is able to identify a small single virus copy within the genome. In addition, we did not observe viral integration close to proto-oncogenes ruling out pB-ALL development based on insertional mutagenesis, providing evidence against direct viral transformation in agreement with observations in human pB-ALL (22).

Published OnlineFirst September 25, 2015; DOI: 10.1158/2159-8290.CD-15-0892

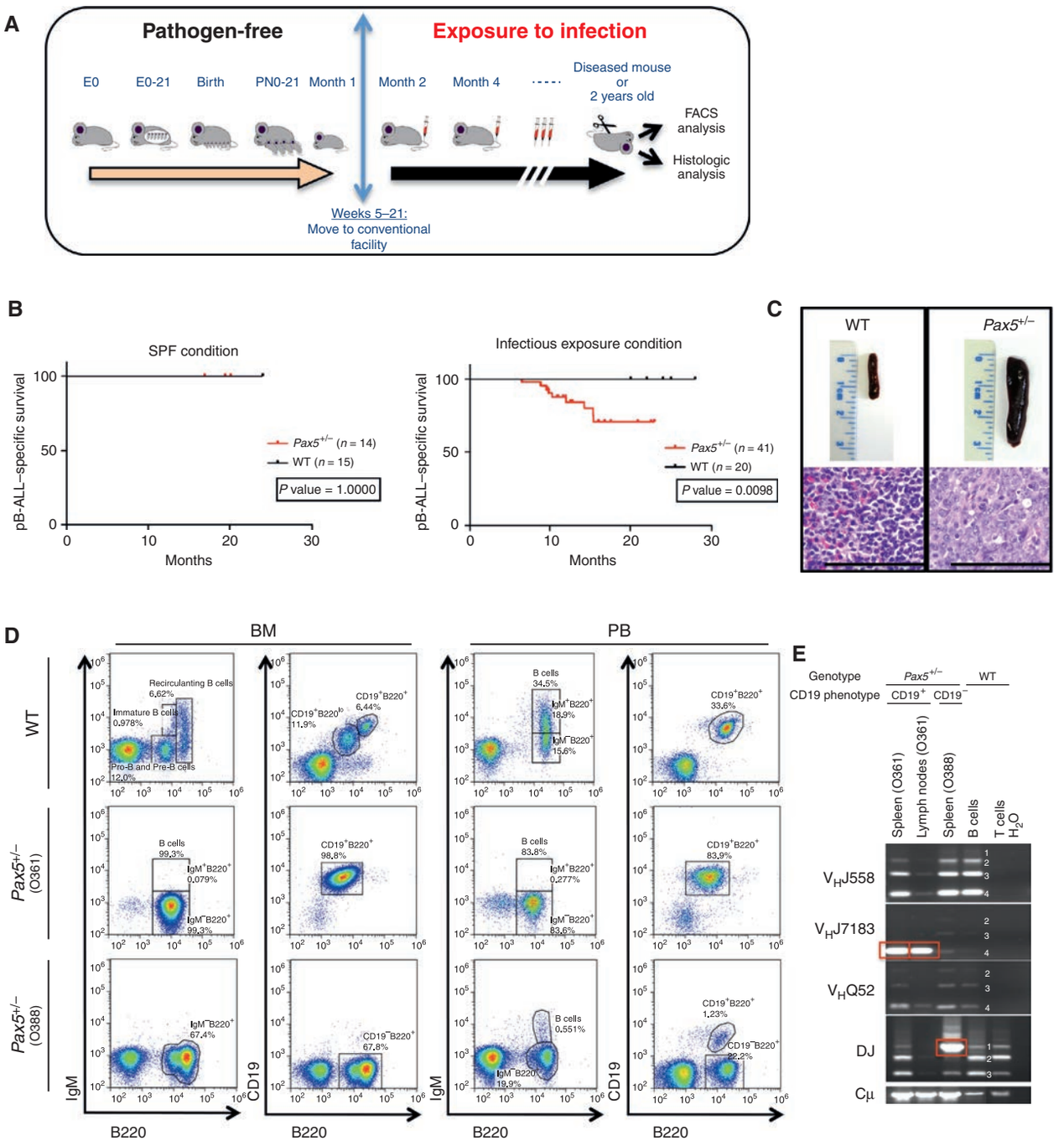

Figure 1. *Pax5* heterozygosity and exposure to infectious stimuli cooperate in pB-ALL development. **A,** experimental setup. Mice are born under SPF conditions and are moved to a non-SPF facility where they are exposed to common infectious pathogens between 5 and 21 weeks after birth. **B,** pB-ALL–specific survival curve of $Pax5^{+/-}$ animals in SPF conditions (red, $n = 14$) compared with WT control mice (black, $n = 15$), close to pB-ALL–specific survival curve of $Pax5^{+/-}$ animals in non-SPF conditions (red, $n = 41$) compared with WT control mice (black, $n = 20$), showing a significantly (log-rank P value 0.0098) shortened life span (right). **C,** example of splenomegaly observed in 55% (5 of 9) of $Pax5^{+/-}$ mice. WT mouse spleen is shown for reference. Hematoxylin and eosin staining of spleen sections from WT- and tumor-bearing $Pax5^{+/-}$ mice shows infiltrating blast cells. Scale bar, 10 μm (= 400×; $n = 9$). **D,** flow cytometric analysis of hematopoietic subsets in diseased $Pax5^{+/-}$ mice. Representative plots of cell subsets from the BM and PB show accumulation of blast B cells in $Pax5^{+/-}$ mice ($n = 9$; age, 6–16 months) compared with control littermate age-matched WT mice ($n = 4$; age, 8–16 months). **E,** immunoglobulin clonality in $Pax5^{+/-}$ tissues infiltrated with blast B cells. PCR analysis of immunoglobulin heavy-chain gene rearrangements in infiltrated spleens and lymph nodes of diseased $Pax5^{+/-}$ mice. Thymocytes (T cells) were included as a negative control, and sorted $CD19^+$ B cells (B cells) from the spleens of healthy mice serve as a control for polyclonal BCR rearrangements (indicated by numbers 1–4). Infiltrated tissues show an increased clonality within their immunoglobulin repertoire (red squares; $n = 2$).

Published OnlineFirst September 25, 2015; DOI: 10.1158/2159-8290.CD-15-0892

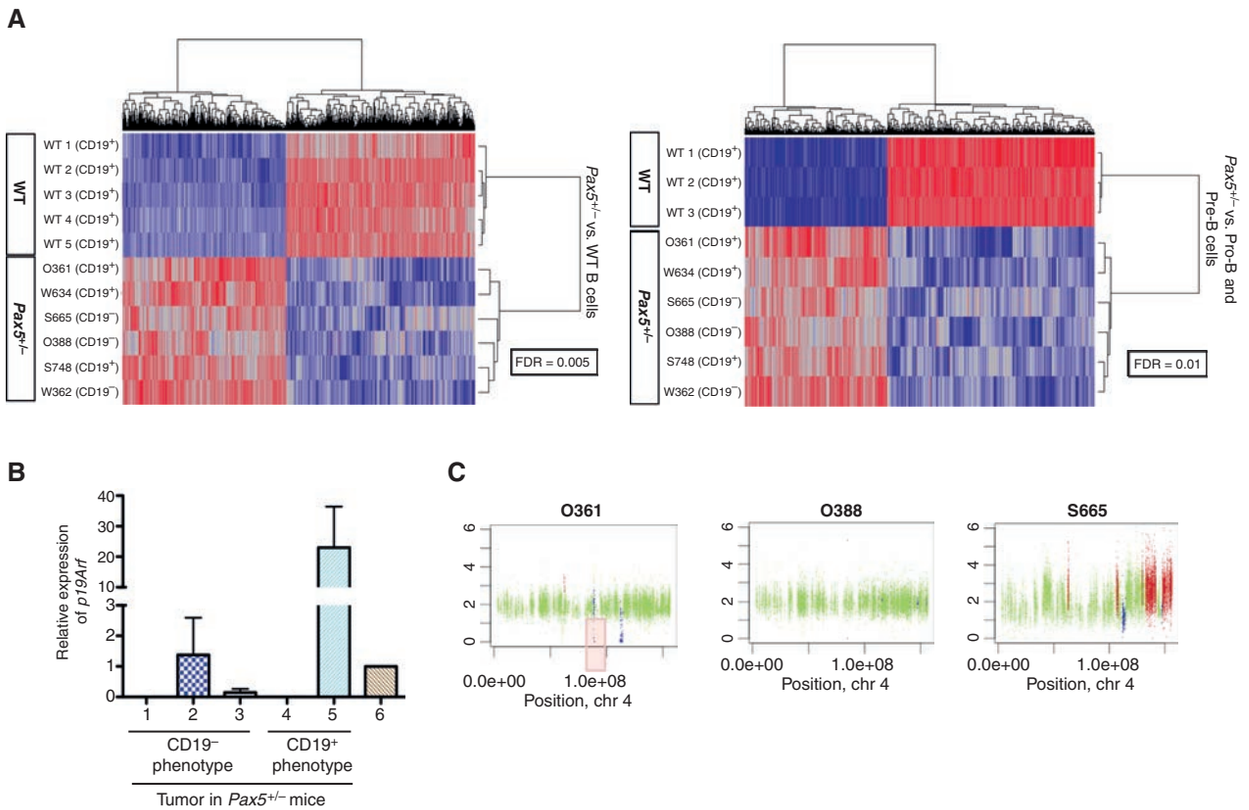

Figure 2. pB-ALLs from *Pax5*$^{+/-}$ mice resemble human pB-ALL. **A,** differential gene expression analysis of tumor-bearing BMs of three *Pax5*$^{+/-}$ mice (O361, W634, and S748 CD19^{+} phenotype; S665, O388, and W362 CD19^{-} phenotype) compared with B220^{+} BM B cells from five WT mice shows significant differences (left). In the right plot, differential gene expression analysis of tumor-bearing BMs of six *Pax5*$^{+/-}$ mice compared with BM pro-B and pre-B cells from three WT mice shows significant differences (FDR = 0.01). **B,** relative expression of *p19Arf* from BM tumor cells of *Pax5*$^{+/-}$ mice (samples 1–5). Total BM of a SCA1-BCR-ABL-p210 mouse was used as a positive control (sample 6). Blast cells of *Pax5*$^{+/-}$ mice 1, 2, and 3 are CD19^{-}, and blast cells of *Pax5*$^{+/-}$ mice 4 and 5 are CD19^{+}. Error bars represent the mean ± SD of three replicates. **C,** loss of *Cdkn2a* locus from all tumor/reference pairs. Copy-number variation profiles were calculated using Free copy number and genotype caller (FREEC). Copy-number profiles displayed a loss of heterozygosity at 4:89274500-89276999 in mouse O361.

Table 1. Genotype and phenotype of pB-ALL–bearing *Pax5*$^{+/-}$ mice

	Mouse number	Mouse age at disease (months)	CD19 phenotype	*Jak3* mutation in mouse[a]	*Jak3* mutation (allele frequency)[b]	*JAK3* human homolog	*Pax5* mutation in mouse[a]	*PAX5* human homolog	*Jak1* mutation in mouse[a]
1	O361	8.8	CD19^{+}	R653H	R653H (50%)	R657Q			S645P
2	O388	9.5	CD19^{-}	R653H	R653H (11%)	R657Q			—
3	S665	6.5	CD19^{-}	—	R563H (2%)	R657Q	P80R	P80R	V657F
4	O332	15.3	CD19^{-}	—	—	—			—
5	W495	10.2	CD19^{-}	—	—	—			—
6	S748	14.2	CD19^{+}	V670A	V670A (27%)	V674A	P80L	Not described	—
7	W893	9.8	CD19^{-}	R653H	R653H (49%)	R657Q			—
8	S767	15.3	CD19^{+}	R653C	R653C (63%)	R657Q			—
9	W634	12	CD19^{+}	R653H	R653H (35%)	R657Q			—

[a]Mutations confirmed by Sanger sequencing.
[b]Mutations confirmed by deep sequencing.

Published OnlineFirst September 25, 2015; DOI: 10.1158/2159-8290.CD-15-0892

Pax5$^{+/-}$ Creates an Aberrant, IL7-Sensitive Precursor B-cell Compartment

We next aimed to explain the mechanism of this specific pB-ALL susceptibility due to *Pax5* heterozygosity under exposure to infections. To this end, the different B-cell developmental stages were analyzed in WT and preleukemic *Pax5*$^{+/-}$ littermates of the same breeding. *Pax5*$^{+/-}$ mice presented a significantly reduced amount of total B cells in the PB when compared with WT mice (Fig. 3A; Supplementary Table S4). This decrease was not induced by the exposure to common pathogens, as a similar decrease in PB B cells was observed in *Pax5*$^{+/-}$ mice housed in an SPF environment (Fig. 3B). On the other hand, we observed significantly higher proportions of (pro+pre)-B and immature B cells in the BM of *Pax5*$^{+/-}$ mice compared with age-matched WT littermates (Fig. 3A; Supplementary Table S4), but no differences were detected in earlier developmental compartments of the BM (data not shown). These data therefore suggest that *Pax5* heterozygosity favors the appearance of an aberrant B-cell precursor compartment in the BM and that differentiation to mature PB B cells is impaired *in vivo* in keeping with observations in *Pax5*-null mice (13) and in a stable *in vivo Pax5* knockdown model (23). These observations are in agreement with reports of preleukemic activity in mice bearing pB-ALL–associated oncogenes, e.g., the *ETV6–RUNX1* fusion (24, 25). The murine precursor B cells are dependent on intact IL7/IL7R signaling and subsequent activation of JAK3 and STAT5 phosphorylation. Thus, we next explored the response of *Pax5*$^{+/-}$ pro-B cells to IL7 withdrawal and showed that *Pax5*$^{+/-}$ pro-B cells are more sensitive to IL7 withdrawal than their WT counterparts (Fig. 3C). Similar observations were obtained when preleukemic *Pax5*$^{+/-}$ pro-B cells were exposed to specific JAK1/3 inhibitors (Fig. 3D). Taken together, these results imply that aberrant precursors present in *Pax5*$^{+/-}$ mice are extremely sensitive to IL7 withdrawal and susceptible for second hits leading to leukemia development.

Mouse Tumor Exome Sequencing Data Identify the Second Hit within the IL7R/JAK3/STAT5 Axis

In order to identify the second hit related to pB-ALL disease with prenatal initiation triggered by infection exposure in the context of impaired B-cell development, we next performed whole-exome sequencing of three *Pax5*$^{+/-}$ tumors and corresponding germline samples on a HiSeq 2500 (Illumina) platform. *Pax5*$^{+/-}$ tumor cells were derived from BM of diseased mice. We identified between 28,638 and 31,105 single-nucleotide variations (SNV) in tumor samples and between 27,141 and 31,151 SNVs in germline samples,

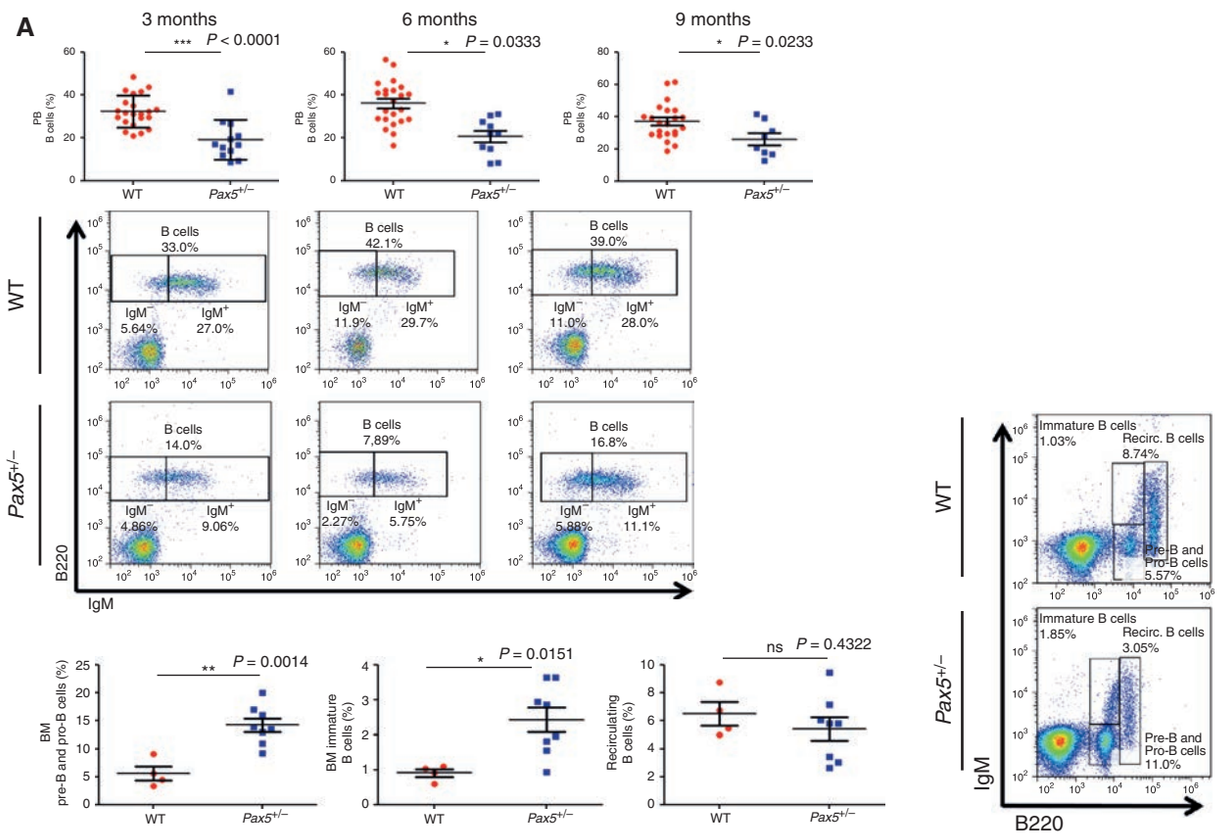

Figure 3. B-cell development in young *Pax5*$^{+/-}$ mice. **A,** percentage of PB B cells (B220^{+}IgM$^{+/-}$) at different time points in *Pax5*$^{+/-}$ mice ($n = 12$) compared with WT mice ($n = 22$) analyzed by flow cytometry. A significant decrease in PB B cells can be observed in *Pax5*$^{+/-}$ mice at 3, 6, and 9 months of age. Error bars represent the SD. *t* test *P* value is indicated in each case. Four-month-old *Pax5*$^{+/-}$ mice ($n = 8$) show increased numbers of pre-B/pro-B cells (B220^{low}IgM^{-}) and immature B cells (B220^{low}IgM^{+}) compared with age-matched WT mice ($n = 4$) but not recirculating B cells (B220^{++}IgM^{+}). Unpaired *t* test *P* value is indicated in each case. (*continued on next page*)

Published OnlineFirst September 25, 2015; DOI: 10.1158/2159-8290.CD-15-0892

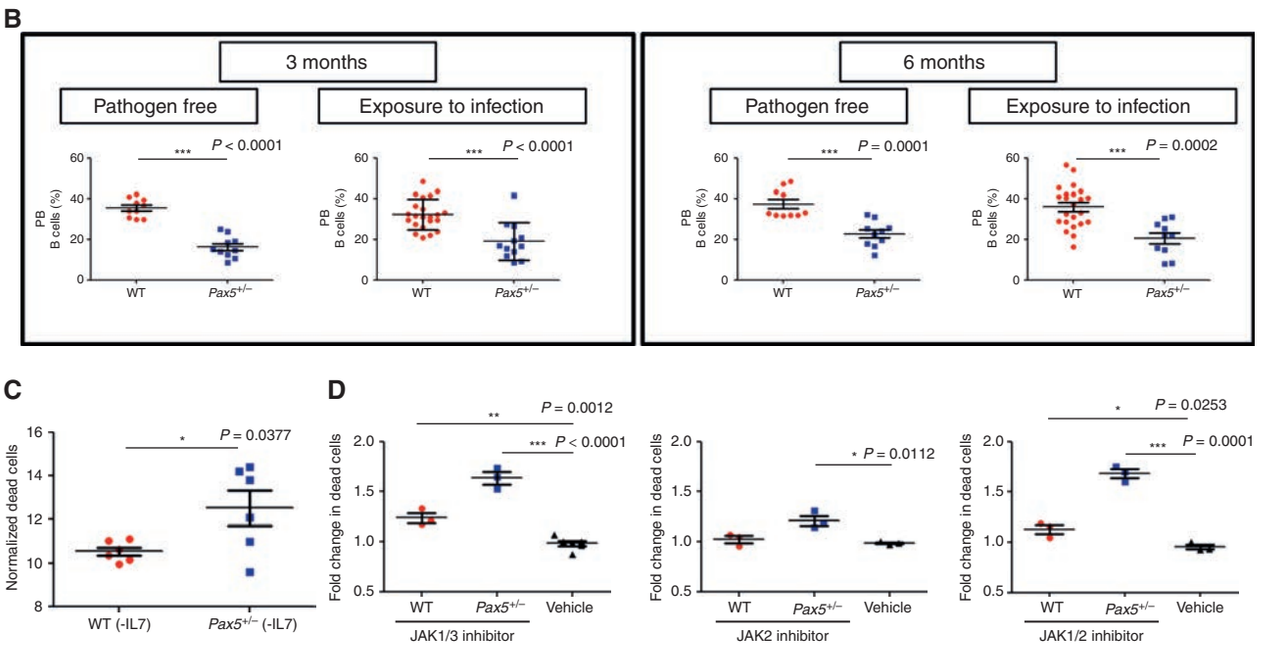

Figure 3. ***(Continued)*** **B,** decrease in PB B cells in *Pax5*$^{+/-}$ mice housed in SPF conditions. Percentage of PB B cells in *Pax5*$^{+/-}$ mice ($n = 10$) compared with WT mice ($n = 10$) analyzed by flow cytometry as B220^{+}IgM$^{+/-}$ cells at 3 and 6 months of age. Error bars represent the mean ± SD. Unpaired *t* test *P* value is indicated in each case. A significant decrease in PB B cells can be observed in *Pax5*$^{+/-}$ mice housed in SPF conditions. **C,** cell death susceptibility mediated by IL7 removal in *Pax5*$^{+/-}$ pro-B cells. Sorted B220^{+} cells from BM of young *Pax5*$^{+/-}$ and WT mice were cultured under conditions to allow the isolation and expansion of a pure population of pro-B cells. Pro-B cells were cultured with or without IL7 for 24 hours. Induction of apoptosis was assessed by flow cytometry using Annexin V/PI staining. Data represent the mean ± SD of normalized apoptotic cells from six independent experiments. Unpaired *t* test *P* value is indicated in each case. **D,** cell death mediated by JAK inhibitors in WT and *Pax5*$^{+/-}$ pro-B cells. IL7-dependent pro-B cells were cultured with tofacitinib (JAK1/3 inhibitor; 1 μmol/L), TG101348 (JAK2 inhibitor; 1 μmol/L), and ruxolitinib (JAK1/2 inhibitor; 1 μmol/L) for 24 hours. Induction of apoptosis was assessed by flow cytometry using Annexin V/PI staining. Graphs indicate the fold change of dead cells treated with the inhibitor in each experiment compared with cells treated with the vehicle. Data represent the mean ± SD from three independent experiments. Unpaired *t* test *P* value is indicated in each case.

resulting in 31 (O361; CD19^{+}), 17 (O388; CD19^{-}), and 9 (S665; CD19^{-}) somatic SNVs in the three mice. Finally, we detected *Jak3* c.1958G>A (p. R653H) as one recurrent heterozygous nonsynonymous somatic SNV in the pseudokinase domain of JAK3 in two mice (Fig. 4A; Supplementary Table S5). The corresponding human homolog (*JAK3*^{R657Q}) is recorded in the cancer gene consensus database (ref. 26; Table 1). Next, we applied Sanger sequencing to the remaining tumors and, surprisingly, we identified nonsynonymous *Jak3* mutations in 6 of 9 mice causing *Jak3*^{R653H} (4/9; human homolog *JAK3*^{R657Q}), *Jak3*^{R653C} (1/9; human homolog *JAK3*^{R657Q}), and *Jak3*^{V670A} (1/9; human homolog *JAK3*^{V674A}; data not shown). This result and the fact that all *Jak3* variants (R653H, R653C, and V670A) are located in a region highly conserved across different species together indicate that these variants are relevant for leukemia evolution (Table 1). We next performed deep sequencing with a depth between 600,000 and 2.5 × 10^{6} reads per *Jak3* SNV and observed the nonsynonymous *Jak3* variant only in tumor samples but not in BM cells of healthy *Pax5*$^{+/-}$ or WT mice (Fig. 4B). In addition, in mice S748 (*Jak3*^{V670A}), W634 (*Jak3*^{R653H}), and S767 (*Jak3*^{R653C}), we were able to monitor leukemia evolution over time by collecting peripheral blood mononuclear cells (PBMC) at routine intervals after birth using deep sequencing at the same depth as described above. All *Jak3* variants were first detectable by deep sequencing and Sanger sequencing when the mouse appeared clinically ill with pB-ALL (Fig. 4C). This result is incompatible with a model in which *Jak3* mutations are present in few cells from birth on and become selected over time. Instead, they are *de novo* mutations occurring on the *Pax5*$^{+/-}$ background as a consequence of environmentally driven selection pressure with a very short latency to leukemia outgrowth.

Somatic *Jak3* Mutations Rescue IL7-Sensitive *Pax5*$^{+/-}$ Precursor B Cells and Cause Leukemia Outgrowth

The corresponding human *JAK3*^{R657Q} and *JAK3*^{V674A} variants result in constitutive kinase activity of JAK3 and downstream STAT5 phosphorylation (27, 28). Hence, we transfected IL3-dependent Ba/F3 cells with the murine *Jak3*^{R653H} variant and observed cytokine-independent growth (Fig. 4D), consistent with phosphorylation of STAT5 in the absence of IL3 (Fig. 4E). Similarly, we observed STAT5 phosphorylation in the mouse leukemic cells carrying *Jak3*^{V670A} (Fig. 4F). Consistently, tumor pro-B cells harboring *Jak3*^{V670A} and *Jak3*^{R653H} grow independent of IL7 (Fig. 4G, H, and I). In two pB-ALLs (O361 and S665), we additionally identified *Jak1* mutations (Table 1). JAK3 pseudokinase mutants are dependent on JAK1 kinase activity for cellular transformation (29). This is consistent with the increase in cell death after administration of the JAK1/2 inhibitor ruxolitinib *in vitro* (Fig. 4J) as well as the decrease in leukemic cell burden *in vivo* (see below).

Published OnlineFirst September 25, 2015; DOI: 10.1158/2159-8290.CD-15-0892

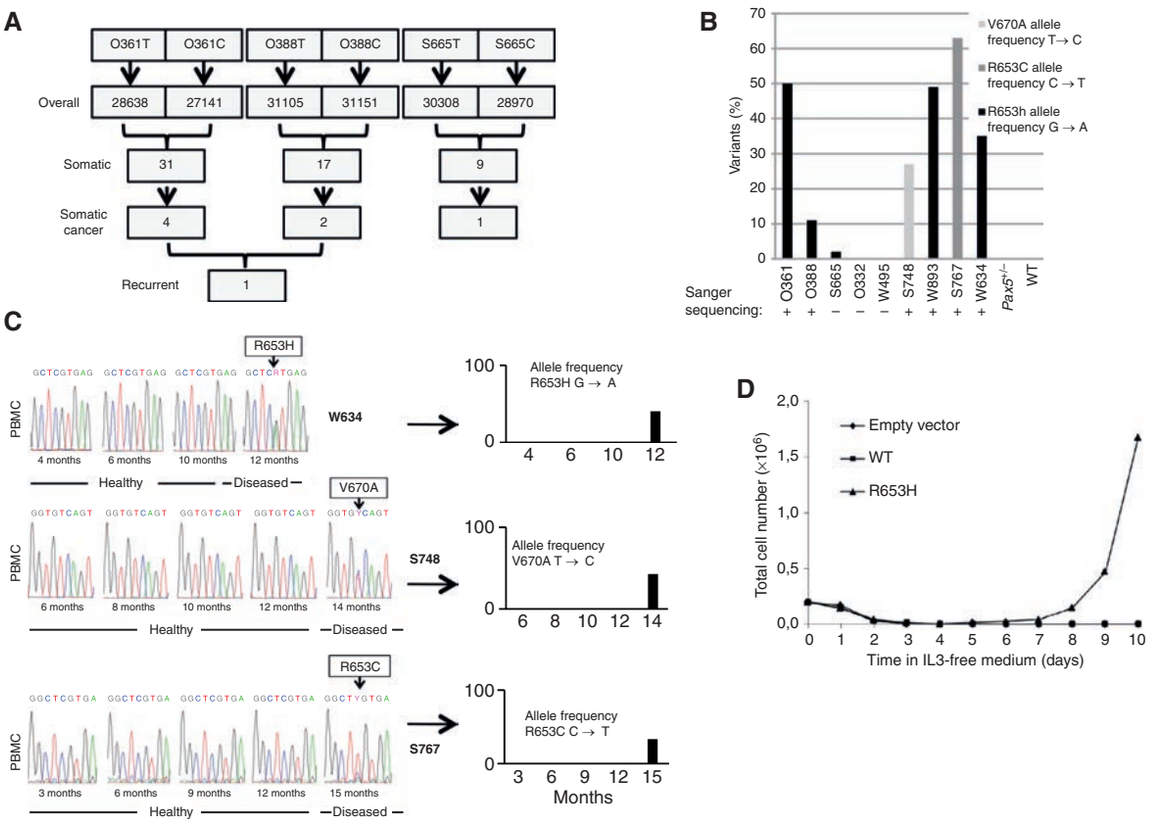

Figure 4. Mouse tumor exome sequencing data identify the second hit within the IL7R/JAK3/STAT5 axis. **A,** exome sequencing analysis yielded around 30,000 SNVs genome wide; 1 to 4 were deemed tumor-specific by MUTECT analysis with one recurring *Jak3* variant. **B,** the allele frequency of the *Jak3* variants V670A, R653C, and R653H is shown for 9 *Pax5*$^{+/-}$ mice. Healthy *Pax5* heterozygous and WT mice serve as negative controls. Variants confirmed by Sanger sequencing are marked +. **C,** backtracking of the mutations *Jak3*^{R653H}, *Jak3*^{V670A}, and *Jak3*^{R653C} by Sanger sequencing and deep sequencing in the PB of *Pax5*$^{+/-}$ mice W634, S748, and S665 ($n = 2$). **D,** Ba/F3 cells were transfected with pMC3 empty vector, pMC3-JAK3^{WT}, or pMC3-JAK3^{R653H}, and hygromycin-resistant cells were selected. Cells were cultured in media without IL3, and their proliferation was measured every day using Trypan Blue. Values represent the mean ($n = 2$) with essentially identical datasets. (*continued on next page*)

To identify the tumor repopulating cells of the murine *Pax5*$^{+/-}$ pB-ALL, we transplanted primary myeloid cells, *Pax5*$^{+/-}$ pro-B cells harboring WT *Jak3*, and *Pax5*$^{+/-}$ pro-B cells harboring *Jak3*^{V670A}, respectively, into sublethally irradiated syngeneic recipient mice. Each of the mice transplanted ($n = 9$) with 10^5 *Pax5*$^{+/-}$ pro-B cells harboring *Jak3*^{V670A} cells developed a pB-ALL with a latency of 13 ± 3 days. The disease was phenotypically identical to the primary disease. In contrast, when recipient mice were transplanted with myeloid cells ($n = 7$; 10^6 cells per mouse) and *Pax5*$^{+/-}$ pro-B cells ($n = 10$; 10^5 cells per mouse), they were incapable of inducing pB-ALL in secondary recipients (Fig. 5A–C). This indicates that infection-induced *Pax5*$^{+/-}$ pB-ALL in this model is propagated by transformed *Pax5*$^{+/-}$ pro-B cells harboring *Jak3*^{V670A} but not *Pax5*$^{+/-}$ pro-B cells harboring WT *Jak3*, and confirms that *Jak3*^{V670A} can induce pB-ALL in mice. These results suggested that the *Pax5* heterozygous condition can establish the environment for the generation of the *Jak3* mutation and is not playing a role in the pathogenesis of the final leukemia. Thus, we next examined the PAX5-independent potential role of the identified *Jak3* mutations in leukemogenesis by injecting 10^6 Ba/F3 cells expressing either *Jak3*^{V670A} ($n = 5$) or *Jak3*^{R653H} ($n = 4$) mutants in nude mice, and we monitored the pB-ALL development by periodic analysis of the presence of blast cells in PB. The results show that both mutants are able to generate pB-ALL in mice with a disease latency of 27 ± 3 days (Supplementary Fig. S3A–S3C), suggesting that inactivating mutations in *Pax5* promote leukemogenesis by simply creating an aberrant IL7-sensitive progenitor compartment that is susceptible to malignant transformation through accumulation of secondary *Jak3* mutations as a rescue mechanism of IL7/IL7R/STAT5 signaling.

Successful *In Vivo* Treatment of *Pax5*$^{+/-}$ pB-ALL Using JAK Inhibitors

These results suggest that JAK1/3 inhibitors may be useful therapeutic options for pB-ALL in patients with germline *PAX5* mutations. Thus, we treated tumor pro-B cells (*Jak3*^{V670A}) with three different selective JAK inhibitors: tofacitinib (JAK1/3), TG101348 (JAK2), and ruxolitinib (JAK1/2). Tumor pro-B cells were sensitive to the JAK1/3 and the JAK1/2 inhibitors but not to the JAK2 inhibitor *in vitro* (Fig. 4J).

We next tested the efficacy of the JAK inhibitors *in vivo*. To this end, mice infused with transformed *Pax5*$^{+/-}$ pro-B cells harboring *Jak3*^{V670A} were randomized to treatment at day 12 when the disease was confirmed by the presence of

Published OnlineFirst September 25, 2015; DOI: 10.1158/2159-8290.CD-15-0892

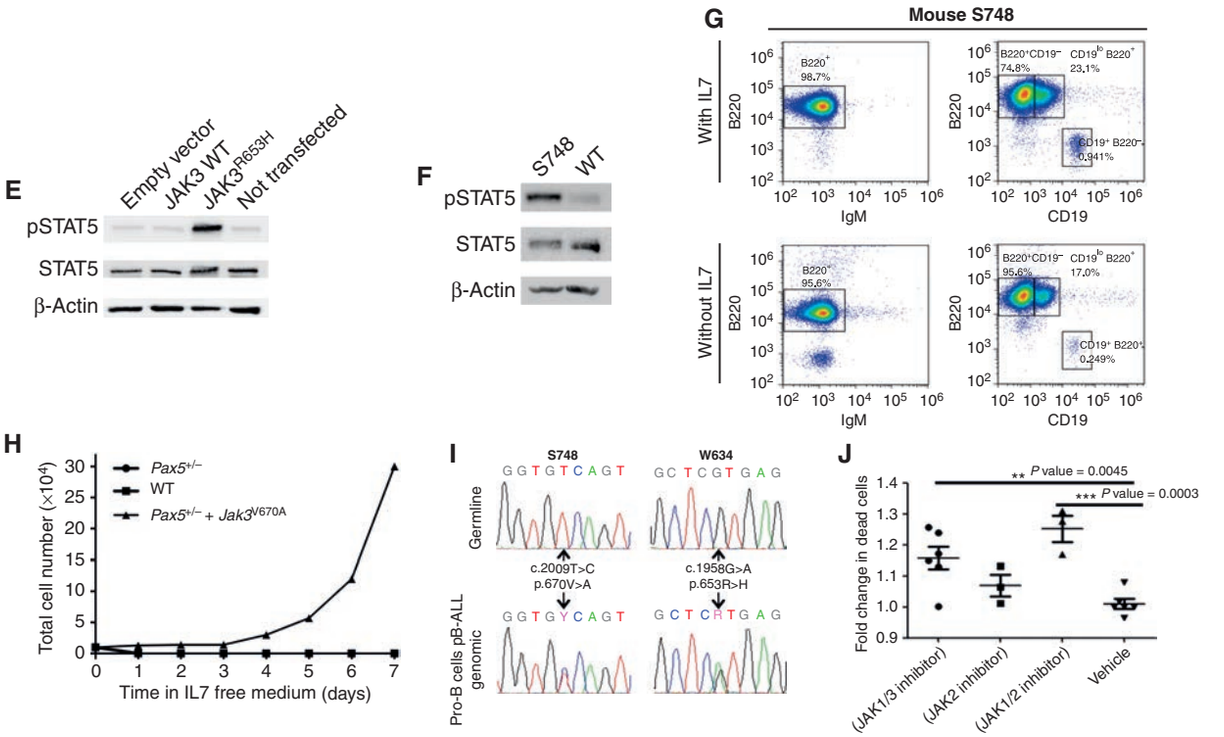

Figure 4. ***(Continued)*** **E,** transfected cells were cultivated in media without IL3 and serum for 4 hours, before being subjected to immunoblot analysis for phosphorylated (p) STAT5, as well as total STAT5 and β-actin as loading controls ($n = 2$, shown is one representative experiment). **F,** lysate of spleen tumor cells (S748), harboring *Jak3*^{V670A}, was subjected to immunoblot analysis for pSTAT5, total STAT5, and β-actin. Tumor cells show constitutive pSTAT5 activation ($n = 2$). **G,** immunophenotype of tumor *Pax5*$^{+/-}$ pro-B cells harboring *Jak3*^{V670A}. Sorted B220$^+$ cells from BM of the diseased *Pax5*$^{+/-}$ mouse were cultured under conditions to allow the isolation and expansion of a pure population of pro-B cells and grow in the absence of IL7 due to the activating *Jak3*^{V670A} mutation. **H,** WT, *Pax5*$^{+/-}$, and *Pax5*$^{+/-}$ *Jak3*^{V670A} primary pro-B cells were cultured in media without IL7. Proliferation was measured using Trypan Blue. Values represent the mean out of three replicates with essentially identical datasets. **I,** Sanger sequencing of leukemic pro-B cells of mice S748 and W634, grown *in vitro* without IL7, validating the variants *Jak3*^{V670A} and *Jak3*^{R653H}, respectively ($n = 2$). **J,** tumor *Pax5*$^{+/-}$ pro-B cells harbor the *Jak3*^{V670A} mutation and grow independently of IL7. Pro-B cells were cultured with tofacitinib (1 μmol/L), TG101348 (1 μmol/L), and ruxolitinib (1 μmol/L) for 24 hours. Induction of apoptosis was assessed by flow cytometry using Annexin V/PI staining. Graph indicates the fold change of dead cells in each experiment. Data represent the mean ± SD from at least three independent experiments. Unpaired *t* test *P* value is indicated.

blast cells in the PB of the reconstituted mice (Fig. 6A). Mice were treated with ruxolitinib for only 5 days. FACS analysis of the PB was used to verify disease remission after therapy. Although ruxolitinib provided no significant survival advantage, all mice treated ($n = 5$) showed a transient decrease in the blast cells (Fig. 6B). However, disseminated leukemia, documented by clinical criteria and FACS (Fig. 6C and D), invariably ensued, except in 1 of 5 mice that was alive and healthy 33 days after discontinuation of treatment, when the mouse was sacrificed, and FACS analysis confirmed that blast cells were not present in the BM (Supplementary Fig. S3D). In summary, these data further suggest that *Jak3* mutations retain driver functions in established leukemia. Thus, targeting the deregulated JAK–STAT pathway could be a promising therapy for this disease.

DISCUSSION

The common belief in childhood pB-ALL development is that children with intrinsic genetic susceptibility to pB-ALL development acquire additional chromosomal aberrations, i.e., *ETV6–RUNX1*—most of them *in utero* during fetal hematopoiesis—as a primary pathogenetic event followed by a broad range of secondary mutational events resulting in a full-blown leukemia. Common among these secondary events are alterations disrupting the *PAX5* gene, which encodes a master transcriptional regulator of B-cell development (13, 14). In this setting, PAX5 seems to retain driver functions in established leukemia because restoring endogenous PAX5 expression triggers disease remission (23).

Recent discoveries of inherited mutations of *PAX5* in a new syndrome of susceptibility to pB-ALL have extended the role of *PAX5* alterations in the pathogenesis of pB-ALL (5, 6). The presence of the inherited mutations of *PAX5* seems to produce a persistent and hidden preleukemic clone that may convert to pB-ALL in only a fraction of the family members (5, 6). The patients lose the WT *PAX5* allele related to a secondary structural aberration of chromosome 9p. In mice, we face the same scenario, but the sequence is reverse. The mice have lost one WT *Pax5* allele and acquire *Pax5* point mutations as secondary events. However, the final common path in both species is reduced transcriptional activity of PAX5. The mechanisms responsible for the conversion of the preleukemic clone, carrying the inherited mutations of *PAX5*,

Published OnlineFirst September 25, 2015; DOI: 10.1158/2159-8290.CD-15-0892

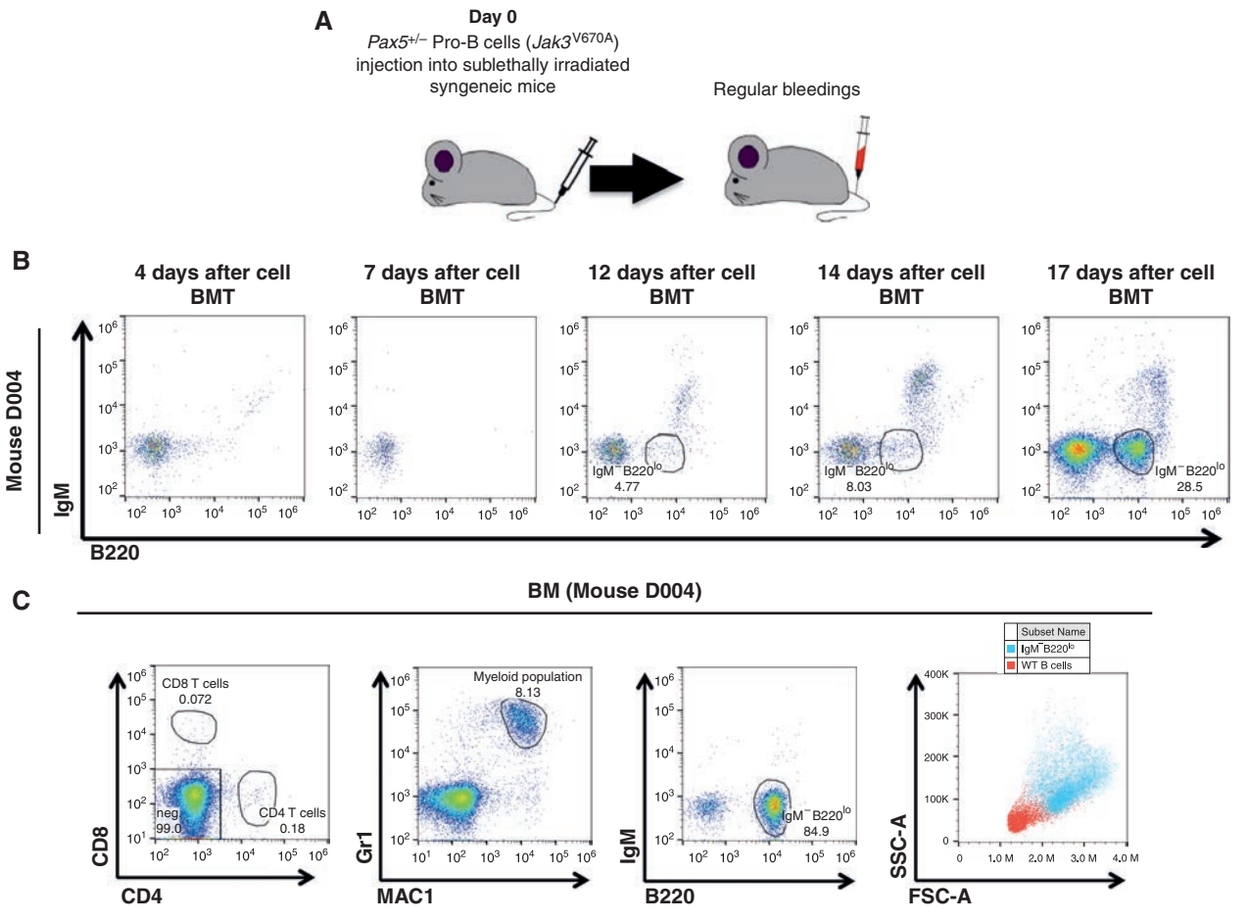

Figure 5. pB-ALL is transplantable to secondary recipients. **A,** experimental setup. A total of 100,000 leukemic *Pax5*$^{+/-}$ pro-B cells harboring *Jak3*^{V670A} mutation were injected into sublethally irradiated WT syngeneic mice. Regular bleedings were performed in order to monitor the development of the pB-ALL. **B,** representative flow cytometric analysis of mice injected with leukemic *Pax5*$^{+/-}$ proB cells harboring *Jak3*^{V670} mutation. Cytometric analyses at different time points show that leukemic pB-ALL cells (B220^{lo}IgM^{-}) were able to grow in secondary recipients. BMT, bone marrow transplant. **C,** representative flow cytometric analysis of mice injected with leukemic *Pax5*$^{+/-}$ proB cells harboring *Jak3*^{V670A} mutation shows the accumulation of pB-ALL cells (B220^{lo}IgM^{-}) in BM. FSC-A, forward scatter-area; SSC-A, side scatter-area.

into pB-ALL are not understood yet. However, recent results suggest that the B-cell–specific enzyme AID is supposed to be the predominant driver of clonal evolution in human ETV6–RUNX1 pB-ALL (30–32) and B-cell lymphoma (33). These observations are in line with previous studies showing that AID is capable of initiating aberrant genomic alterations in precursor B cells (34) The pB-ALL that originated as a result of delayed infection exposure in *Pax5*$^{+/-}$ mice offers a unique possibility to confirm if the proposed mechanisms are involved in the conversion of the preleukemic clone into a full-blown leukemia (35, 36). The assumption of a functional interaction between inherited susceptibility and postnatal infection is a highly attractive explanation in the natural history of childhood ALL. Our results bring strong functional proof in support of the "infectious" hypothesis that posits that exposure to infection represents an oncogenic environment that promotes leukemia development. In our experimental model, *Pax5*$^{+/-}$ mice never develop leukemia in a pathogen-free environment. However, exposure of *Pax5*$^{+/-}$ mice to infectious stimuli at the age of 2 to 5 months represents the necessary oncogenic environment. Hence, this observation closely mimics the human situation. Children encounter a plethora of different infectious agents at the ages of 2 to 5 years, but all attempts to identify a single consistent infectious agent have failed in humans with pB-ALL (11). This indicates that it is a sequence of infections and broad immune responses in an unprimed immune system, which is important for leukemia development, rather than exposure to a single pathogen. Likewise, several months prior to ALL, children show a marked deterioration of immune response and profound liability to a variety of infections (35).

In our model, inactivating mutations in *Pax5* promote leukemogenesis by creating an aberrant IL7-sensitive progenitor compartment. This progenitor population is susceptible to malignant transformation through accumulation of secondary *Jak3* mutations on the basis of a selection pressure triggered by the increased and recurrent exposure to delayed infection in conventional housing facilities. These somatic *Jak3* mutations induce leukemia with a phenotype very similar to the human pB-ALL linked to germline mutations

Published OnlineFirst September 25, 2015; DOI: 10.1158/2159-8290.CD-15-0892

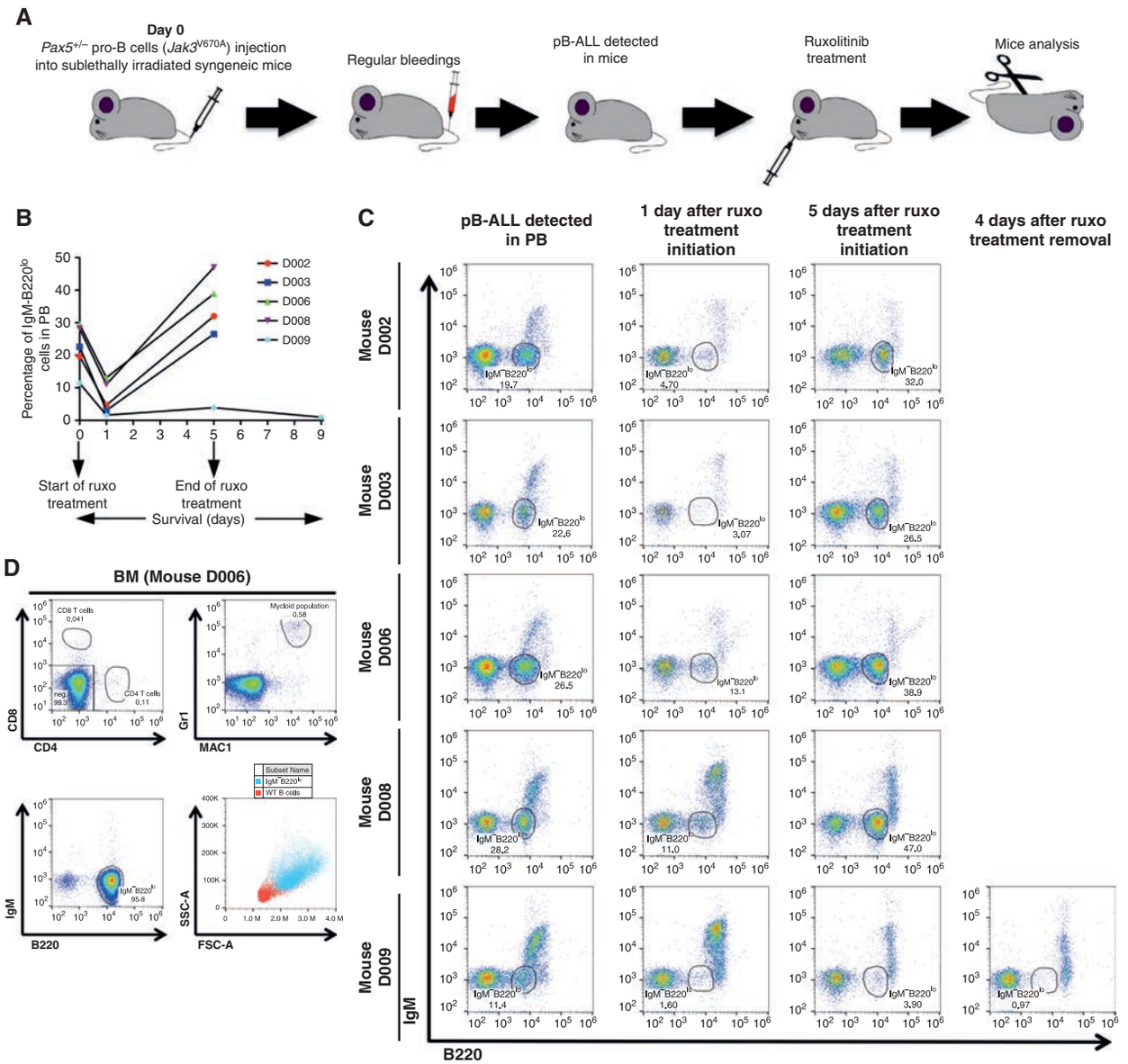

Figure 6. *In vivo* efficacy of JAK inhibition in transformed *Pax5*$^{+/-}$ pro-B cells harboring *Jak3*^{V670A}. **A,** experimental setup. A total of 100,000 leukemic *Pax5*$^{+/-}$ pro-B cells harboring *Jak3*^{V670A} mutation were injected into sublethally irradiated WT syngeneic mice. Regular bleedings were performed in order to check the development of the pB-ALL. When pB-ALL cells (B220^{lo}IgM^{-}) were detected in the PB, the mouse treatment with ruxolitinib started. Mice were treated with ruxolitinib for only 5 days. FACS analysis of the PB was used to verify disease remission after therapy. **B,** percentage of PB pB-ALL cells (B220^{lo}IgM^{-}) was monitored by flow cytometry at different time points in mice treated with ruxolitinib (ruxo). **C,** follow-up of leukemic cells (B220^{lo}IgM^{-}) by PB flow cytometry in mice before and after ruxolitinib treatment. Mice treated with ruxolitinib showed a transient decrease in the blast cells except in mouse D009, which was alive and healthy 33 days after discontinuation of treatment. **D,** representative disseminated leukemia documented by FACS analysis of the BM of mice 5 days after starting treatment with ruxolitinib.

in *PAX5* with respect to clinical, immunophenotypic, and molecular genetic characteristics. *In vivo* transplantation experiments demonstrate that the activating *Jak3* mutations *per se* are sufficient to drive leukemia. Thus, targeting the deregulated JAK–STAT pathway can be a promising therapy for this disease, as we have shown *in vivo*.

Strikingly, this model parallels very well the incomplete penetrance observed in human *PAX5*$^{+/-}$ leukemia. Further studies with *Pax5*$^{+/-}$ mice exposed to the same infectious conditions *in utero* and in the first month of their life will reveal if the timing and pattern of infectious exposure are indeed relevant for pB-ALL development. This suggestion was rendered moot over 70 years ago (37). Toward this development, our findings are important not only for endorsing the credibility of the "infectious" hypothesis, but also for encouraging the prospect of novel interventions that might help to prevent a significant proportion of childhood leukemia.

Published OnlineFirst September 25, 2015; DOI: 10.1158/2159-8290.CD-15-0892

METHODS

Heterozygous Pax5$^{+/-}$ *Mice*

The heterozygous *Pax5*$^{+/-}$ mice (15) have been described previously. *Pax5*$^{+/-}$ and control WT mice were born and kept at the SPF facility until exposed to a common infectious environment. All animal work was conducted according to relevant national and international guidelines, and it has been approved by the Bioethics Committee of the University of Salamanca and by the Bioethics Subcommittee of Consejo Superior de Investigaciones Cientificas (CSIC). Both male and female WT and *Pax5*$^{+/-}$ mice of a mixed C57BL/6 × CBA background were included in the study. We used WT and *Pax5*$^{+/-}$ littermates of the same breeding. Upon signs of disease, mice were sacrificed and subjected to standard necropsy procedures. All major organs were examined under the dissecting microscope. Tissue samples were taken from homogenous portions of the resected organ and fixed immediately after excision. Differences in Kaplan–Meier survival plots of transgenic and WT mice were analyzed using the log-rank (Mantel–Cox) test.

FACS Analysis

Nucleated cells were obtained from total mouse BM (flushing from the long bones), PB, thymus, or spleen. Contaminating red blood cells were lysed with red cell lysis buffer, and the remaining cells were washed in PBS with 1% fetal calf serum (FCS). After staining, all cells were washed once in PBS and were resuspended in PBS with 1% FCS containing 2 mg/mL propidium iodide (PI) to allow dead cells to be excluded from both analyses and sorting procedures. The samples and the data were acquired in an AccuriC6 Flow Cytometer and analyzed using FlowJo software. Specific fluorescence of FITC, Phycoerythrin, PI, and Allophycocyanin excited at 488 nm (0.4 W) and 633 nm (30 mW), respectively, as well as known forward and orthogonal light scattering properties of mouse cells, were used to establish gates. Nonspecific antibody binding was suppressed by preincubation of cells with CD16/CD32 Fc-block solution (BD Biosciences). For each analysis, a total of at least 50,000 viable (PI$^-$) cells was assessed.

The following antibodies were used for flow cytometry: anti-B220 (RA3-6B2), CD3ε (145-2C11), CD4 (RM4-5; 1:500), CD8a (53-6.7; 1:500), CD11b/MAC1 (M1/70; 1:200), CD19 (1D3), CD117/c-KIT (2B8; 1:200), CD127/IL7Rα (A7R34; 1:50), Ly-6G/Gr1 (RB6-8C5), IgM (R6-60.2), SCA1/Ly-6A/E (E13-161.7; 1:50), CD25 (PC61), CD48 (HM48-1), and CD150 (TC15-12F12.2). Unspecific antibody binding was suppressed by preincubation with CD16/CD32 (2.4G2) Fc-block solution (PharMingen). The different hematopoietic progenitors and B-cell stages were defined by flow cytometry as shown in Supplementary Fig. S2A and S2B. All antibodies were purchased from BD Biosciences and used at a 1:100 dilution unless otherwise indicated.

Histology

Animals were sacrificed by cervical dislocation; tissue samples were formalin-fixed and embedded in paraffin. Pathology assessment was performed on hematoxylin–eosin-stained sections under the supervision of Dr. Oscar Blanco, an expert pathologist at the Salamanca University Hospital.

V(D)J Recombination

Immunoglobulin rearrangements were amplified by PCR using the primers below. Cycling conditions consisted of an initial heat activation at 95°C followed by 31 to 37 cycles of denaturation for 1 minute at 95°C, annealing for 1 minute at 65°C, and elongation for 1 minute 45 seconds at 72°C. This was followed by a final elongation for 10 minutes at 72°C. To determine the DNA sequences of individual V(D)J rearrangements, the PCR fragments were isolated from the agarose gel and cloned into the pGEM-Teasy vector (Promega); the DNA inserts of at least ten clones corresponding to the same PCR fragment were then sequenced. The following primer pairs were used: V_HJ558: forward CGAGCTCTCCARCACAGCCTWCATGCARCTCARC, reverse GTCTAGATTCTCACAAGAGTCCGATAGACCCTGG; V_H7183: forward CGGTACCAAGAASAMCCTGTWCCTGCAAATGASC, reverse GTCTAGATTCTCACAAGAGTCCGATAGACCCTGG; V_HQ52: forward CGGTACCAGACTGARCATCASCAAGGACAAYTCC, reverse GTCTAGATTCTCACAAGAGTCCGATAGACCCTGG; GH: forward TTCAAAGCACAATGCCTGGCT, reverse GTCTAGATTCTCACAAGAGTCCGATAGACCCTGG; and Cμ: forward TGGCCATGGGCTGCCTAGCCCGGGACTT, reverse GCCTGACTGAGCTCACACAAGGAGGA.

Microarray Data Analysis

Total RNA was isolated in two steps using TRIzol (Life Technologies) followed by RNeasy Mini-Kit (Qiagen) purification, following the manufacturer's RNA Clean-up Protocol with the optional On-Column DNase treatment. The integrity and the quality of the RNA were verified by electrophoresis, and its concentration was measured. Samples were analyzed using Affymetrix Mouse Gene 1.0 ST arrays.

Briefly, the robust microarray analysis algorithm was used for background correction, intra- and intermicroarray normalization, and expression signal calculation (38–40). Once the absolute expression signal for each gene (i.e., the signal value for each probe set) was calculated in each microarray, a method called significance analysis of microarray (41) was applied to calculate significant differential expression and find the gene probe sets that characterized the tumor-bearing BM from *Pax5*$^{+/-}$ mice compared with BM-derived B220$^+$ cells from WT mice. The method uses permutations to provide robust statistical inference of the most significant genes and provides *P* values adjusted to multiple testing using FDR (42). A cutoff of FDR < 0.05 was used for the differential expression calculations. We applied all these methods using R and Bioconductor (43).

The data discussed in this publication have been deposited in NCBI's Gene Expression Omnibus (GEO; ref. 44) and are accessible through GEO Series accession number GSE62529.

Enrichment Analysis

Differentially expressed genes were tested for enrichment using GSEA from MSigDB (21). Gene expression signatures that are specifically upregulated or downregulated in human B-ALL gene sets (18, 19) were also assessed for their overlap with those that were upregulated or downregulated within tumor specimens using GSEA. We also carried out more enrichment analysis for the specific normal murine B-cell stage signatures (20). Finally, we carried out one more enrichment analysis for the specific *Pax5* gene signatures described in refs. 23 and 45–47.

Cdkn2a/Arf *Expression*

cDNA was synthesized from BM tumor cells of *Pax5*$^{+/-}$ mice using the High Capacity RNA-to-cDNA Kit and used for TaqMan gene expression assays. For quantitative PCR, the following TaqMan Gene Expression Assay (Applied Biosystems) was used: *Cdkn2a/Arf* (Mm.PT.56a.8388138). *Gadph* (Mm.PT.39a.1) was used as an internal control.

Detection of Viral Integration

The Genome Information Broker for Viruses (GIB-V) was screened for viral sequences. The database comprises the genomes of 25,525 clones and strains of DNA and RNA viruses (mouse and human). The virus detection can be divided into three steps: retrieve potential viral sequences, filter low-quality detections, and analyze paired-end reads for viral integration. Reads, which could not be mapped against the mouse reference genome (GRCm38) with Burrows-Wheeler Aligner

Published OnlineFirst September 25, 2015; DOI: 10.1158/2159-8290.CD-15-0892

(BWA) at default and with Bowtie 2 at high sensitivity (minimum mapping concordance of 85%), are candidates for sequences of other (e.g., viral) origin. Hence, they were further inspected for sequence similarity with genomes in the GIB-V database using Bowtie 2 with the following parameters: bowtie2 –very-sensitive –mp 1,1 –rdg 2,1 –rfg 2,1 –score-min L,0,–0.15.

Reads could be mapped to multiple viruses or strains of the same virus to avoid missing alignments due to sequence similarity between the viral sequences. The viral genomes were analyzed for low complexity and repetitive regions with RepeatMasker and compared with the mouse reference genome with the Nucmer algorithm in the MUMmer package. Low-quality alignments within repeats or regions with high sequence homology with the mouse genome were discarded as well as multiple alignments of one read against the same viral genome. Paired-end reads, where one mate mapped to the mouse genome and the other mate to a virus, hinted at possible viral integration spots. Candidates, like the integration on *Pax5*, were investigated manually with the Integrative Genomics Viewer to pinpoint the exact breakpoints.

Mouse Exome Library Preparation and Next-Generation Sequencing

Sample Acquisition The AllPrep DNA/RNA Mini Kit (Qiagen) was used to purify DNA according to the manufacturer's instructions.

Exome Library Preparation and Next-Generation Sequencing Exome library preparation was performed using the Agilent SureSelectXT Mouse All Exon Kit with modifications. Targeted capture by hybridization to an RNA library was performed according to the manufacturer's protocol. Purification and enrichment of the captured library were achieved by binding to MyOne Streptavidin T1 Dynabeads (Life Technologies) and off-bead PCR amplification in the linear range. Sequencing (2×100 bp) with a 6-bp index read was performed using the TruSeq SBS Kit v3 on the HiSeq 2500 (Illumina).

Data Analysis Fastq files were generated by using BcltoFastq 1.8.4 (Illumina). BWA version 0.7.4. was used to align sequence data to the mouse reference genome (GRCm38.71). Conversion steps were carried out using SAMtools followed by removal of duplicate reads. Local realignment around indels, SNP-calling, annotation, and recalibration was facilitated by GATK 2.4.9. Mouse dbSNP138 and dbSNP for the used mouse strains were used as training datasets for recalibration. Resulting variation calls were annotated by Variant Effect Predictor using the Ensembl database (v70) and imported into an in-house MySQL database to facilitate automatic and manual annotation, reconciliation, and data analysis by complex database queries. Loss-of-function prediction scores for PolyPhen2 and SIFT were extracted from this Ensembl release.

Somatic calls were produced using MuTect (48) and VarScan (49). For VarScan2 results, false-positive filtering as suggested by the author was applied. To clear the resulting file of suspicious-looking results, only entries with at least 9% difference in allele frequency between tumor and normal were kept for further analysis. Cancer-related genes were determined by translating the cancer gene consensus from the Catalogue of Somatic Mutations in Cancer (COSMIC) using Ensembl's BioMart.

Sequencing

Mutations were validated using Sanger sequencing on a 3130 Genetic Analyzer (Applied Biosystems). The following primer pairs were used: *mJak3* forward: CGGGATGTGGGGCTTTAACT, reverse: GCAGACACGGGGTATAGTGG; *mJak1* forward: CCA GACAGCCAGGAGAACAG, reverse: CGTCTGCATAGTACCCACCC; *mPax5* forward: CTCGTACATGCACGGAGACA, reverse: GGAC CCTTCAGTACACCAGC.

Deep Sequencing

For deep sequencing, Illumina TruSeq Adapters were used with the following product-specific primers: *mJak3* R653H/C forward: CCCTGTTCCCTCCTGTAACAC, reverse: AGTGGGACTGACAC CAGGAT; *mJak3* V670A forward: AACGTCTCAGCACGGAAGG, reverse: GTGCAAAGGTGACCATGACAG. Samples were sequenced on a HiSeq 2500 (Illumina Inc.).

Ba/F3 Experiments

Cell Lines Ba/F3 cells were directly obtained from the cell bank DMSZ (ACC 300; Heidelberg). The cells were maintained according to the supplier's instructions, authenticated by the company, and used within 6 months of receipt. Species specificity was documented by PCR, and the cell line was characterized by morphology, FACS analysis, and cytogenetics. No authentication has been done by the authors. Cells were cultivated in RPMI-1640 Medium GlutaMAX (Life Technologies), supplemented with 10% (v/v) heat-inactivated FCS, Gentamycin (50 µg/mL), and recombinant mouse IL3 (10 µg/mL; Life Technologies), at 37 °C and 5% CO_2.

Generation of Murine Jak3^{R653H} A cDNA encoding the coding sequence of the WT murine *Jak3* was obtained from the Riken Full Length cDNA Clone A130091E14 (Source Bioscience) via PCR using the Phusion High-Fidelity DNA Polymerase (Thermo Scientific). The mutant cDNA for murine *Jak3*^{R653H} was created by site-directed mutagenesis by PCR (*mJak3*^{WT} forward: GGCGCACGCGTATGGCACCTCCAAGT GAGG, reverse: CCTCGGGGCCCTCCGGGTCTTCCACGCCAC; *mJak3*^{R653H} forward: CGGAAGGTGCTCCTGGCTCATGAGGGGGGTGATGGG AATC; reverse: GATTCCCATCACCCCCCTCATGAGCCAGGAGCAC CTTCCG). The WT and mutant murine *Jak3* sequences were cloned into a derivative of a bicistronic expression vector (pMC3) used previously for stable expression of genes in cell lines. Here, the vector was modified to encode the Hygromycin resistance gene as the second cistron (pMC3-JAK3.Hygro).

Ba/F3 cells were transfected using the Amaxa Nucleofector Technology (Lonza), according to the manufacturer's protocol. Cells harboring the plasmids were selected using 600 µg/mL Hygromycin B (Life Technologies). To examine the PAX5-independent potential role of the identified *Jak3* mutations in leukemogenesis, we injected Ba/F3 cells expressing either *Jak3*^{V670A} ($n = 5$) or *Jak3*^{R653H} ($n = 4$) in the tail vein of nude mice as previously described (50).

Proliferation Assay

Ba/F3 cells (2×10^5) expressing either murine *Jak3*^{WT}, *Jak3*^{R653H}, or the empty vector control were washed twice with medium without IL3, before they were cultured in the absence of IL3 for 10 days. *Pax5*$^{+/-}$ (*Jak3*^{V670A}), *Pax5*$^{+/-}$, and WT pro-B cells (1×10^4) were washed twice with medium without IL7, before they were cultured in the absence of IL7 for 7 days. Proliferation was measured by counting the cells every day using Trypan Blue (Sigma-Aldrich).

Immunoblot Analysis

Whole-cell extracts were obtained as previously described (28). Spleen samples were prepared using a 100-µm cell strainer and depleted of erythrocytes using NH_4Cl, before lymphocytes were lysed in RIPA buffer (50 mmol/L Tris, pH 8.0, 150 mmol/L NaCl, 0.5% Sodiumdeoxycholate, 1% NP-40 substitute, 0.1% SDS) containing protease and phosphatase inhibitors (Roche Diagnostics). Whole protein (20 µg) was separated on SDS-PAGE and transferred to Hybond-C Extra membranes (Amersham Biosciences). Immunoblotting was carried out using the following antibodies: anti–phospho-STAT5 (1:1,000), anti-STAT5 (1:1,000; Cell Signaling), and anti–β-actin clone AC-74 (1:10,000; Sigma-Aldrich). Detection was

Published OnlineFirst September 25, 2015; DOI: 10.1158/2159-8290.CD-15-0892

done using anti-rabbit or anti-mouse horseradish peroxidase conjugates (Santa Cruz Biotechnology), respectively, with an enhanced chemiluminescence system (Thermo Scientific).

Pro–B-cell Culture

Iscove's Modified Dulbecco's Medium (IMDM) supplemented with 50 μmol/L β-mercaptoethanol, 1 mmol/L L-glutamine, 2% heat-inactivated FCS, 1 mmol/L penicillin–streptomycin (BioWhittaker), and 0.03% (w/v) primatone RL (Sigma) was used for pro–B-cell culture experiments. Pro-B cells isolated by magnetic-activated cell sorting for $B220^+$ (Milteny Biotec) from BM were cultured on Mitomycin C–treated ST2 cells in IMDM medium containing IL7 (R&D Systems). IL7-independent tumor pro-B cells were grown in the same medium without IL7.

Inhibitor Experiments

WT, $Pax5^{+/-}$, and tumor pro-B cells were seeded at 10^6/3 mL/well in 6-well plates and treated with or without (vehicle) tofacitinib (JAK1/3 inhibitor; 1 μmol/L), TG101348 (JAK2 inhibitor; 1 μmol/L), and ruxolitinib (JAK1/2 inhibitor; 1 μmol/L) for 24 hours before being subjected to cell viability assay. Experiments were performed at the same time under the same experimental conditions.

Apoptosis Assays

Aliquots (200 μL) containing 10^6 cells in 10 mmol/L Hepes/NaOH, ph 7.4, 140 mmol/L NaCl, and 2.5 mmol/L CaCl2 were incubated with Annexin V–FITC (BD Biosciences) to a final concentration of 1 μg/mL for 10 minutes, at room temperature in the dark, and then labeled with PI to a final concentration of 2 μg/mL (PI in binding buffer). Flow cytometry was performed within an hour of labeling, and data were analyzed using FlowJo software. The difference between experimental variables was determined using the Student *t* test.

BM Transplantation Experiments

BM myeloid cells, $Pax5^{+/-}$ pro-B cells with intact *Jak3*, and $Pax5^{+/-}$ proB cells harboring the $Jak3^{V670A}$ mutation were injected intravenously into sublethally irradiated (4 Gy) secondary recipient 12-week-old male syngenic mice (C57BL/6 × CBA). Disease development in the recipient mice was monitored by periodic PB analysis until blast cells were detected. Then, they were sacrificed and assessed for pB-ALL development.

Preclinical Therapeutics

Ruxolitinib prepared in PBS was administered at 180 mg/kg, orally, twice a day, when animals had developed a significant leukemic burden as documented by FACS analysis of PB. Disease development in the recipient mice was monitored by periodic PB analysis until blast cells were detected. Then they were sacrificed and assessed for pB-ALL development.

Disclosure of Potential Conflicts of Interest

S.N. Constantinescu has received speakers bureau honoraria from Novartis and Shire New Horizons in Hematology and is a consultant/advisory board member for Dafra, Novartis, Personal Genetics, and Shire. No potential conflicts of interest were disclosed by the other authors.

Authors' Contributions

Conception and design: J. Hauer, C. Vicente-Dueñas, I. Sánchez-García, A. Borkhardt

Development of methodology: A. Martín-Lorenzo, I. González-Herrero, I. García-Ramírez, S. Ginzel, R. Thiele, S.N. Constantinescu, A. Orfao, M.B. García-Cenador, F.J. García-Criado

Acquisition of data (provided animals, acquired and managed patients, provided facilities, etc.): A. Martín-Lorenzo, J. Hauer, C. Vicente-Dueñas, F. Auer, I. González-Herrero, I. García-Ramírez, M. Gombert, D. Schäfer, O. Blanco, A. Orfao, A. Borkhardt

Analysis and interpretation of data (e.g., statistical analysis, biostatistics, computational analysis): A. Martín-Lorenzo, J. Hauer, C. Vicente-Dueñas, F. Auer, I. González-Herrero, I. García-Ramírez, S. Ginzel, R. Thiele, C. Bartenhagen, M. Dugas, M. Gombert, D. Schäfer, A. Mayado, D. Alonso-López, J. De Las Rivas, C. Cobaleda, I. Sánchez-García, A. Borkhardt

Writing, review, and/or revision of the manuscript: A. Martín-Lorenzo, J. Hauer, C. Vicente-Dueñas, F. Auer, I. González-Herrero, I. García-Ramírez, S.N. Constantinescu, D. Schäfer, A. Mayado, A. Orfao, D. Alonso-López, J. De Las Rivas, C. Cobaleda, I. Sánchez-García

Administrative, technical, or material support (i.e., reporting or organizing data, constructing databases): M. Gombert, A. Borkhardt

Study supervision: J. Hauer, C. Vicente-Dueñas, I. Sánchez-García, A. Borkhardt

Acknowledgments

The authors are indebted to all members of their groups for useful discussions and for their critical reading of the manuscript. They are grateful to Dr. Meinrad Busslinger for the $Pax5^{+/-}$ mice. The authors also thank Lorraine Springuel and Jean-Christophe Renauld, Ludwig Cancer Research Brussels, for tofacitinib.

Grant Support

J. Hauer has been supported by the German Children's Cancer Foundation and from the "Forschungskommission" of the medical faculty of the Heinrich Heine University and the "Strategischer Forschungsfond" of the Heinrich Heine University. S. Ginzel has been supported by a scholarship from the Hochschule Bonn-Rhein-Sieg. A. Borkhardt has been supported by the German Children's Cancer Foundation and the Federal Ministry of Education and Research, Bonn, Germany. Funding to S.N. Constantinescu from Salus Sanguinis, Fondation contre le cancer Belgium; Interuniversity Attraction Poles IAP, and ARC 10/15-027 is acknowledged. Research in the I. Sánchez-García group is partially supported by FEDER and MINECO (SAF2012-32810 and Red de Excelencia Consolider OncoBIO SAF2014-57791-REDC), Instituto de Salud Carlos III (PIE14/00066), Junta de Castilla y León (BIO/SA32/14 , BIO/SA51/15, and CSI001U14), Fundacion Inocente Inocente, and the ARIMMORA project [European Union's Seventh Framework Programme (FP7/2007-2013) under grant agreement no. 282891]. The I. Sánchez-García lab is a member of the EuroSyStem and the DECIDE Network funded by the European Union under the FP7 program. A. Borkhardt and I. Sánchez-García have been supported by the German Carreras Foundation (DJCLS R13/26). Research in the C. Vicente-Dueñas group is partially supported by a "Miguel Servet" Grant (CP14/00082 - AES 2013-2016) from the Instituto de Salud Carlos III (Ministerio de Economía y Competitividad). Research at C. Cobaleda's lab was partially supported by FEDER, Fondo de Investigaciones Sanitarias (PI13/00160 and PI14/00025), and from an institutional grant from the Fundacion Ramon Areces. A. Martín-Lorenzo was supported by FSE-Conserjería de Educación de la Junta de Castilla y León (CSI001-13).

The costs of publication of this article were defrayed in part by the payment of page charges. This article must therefore be hereby marked *advertisement* in accordance with 18 U.S.C. Section 1734 solely to indicate this fact.

Received July 23, 2015; revised September 15, 2015; accepted September 17, 2015; published OnlineFirst September 25, 2015.

REFERENCES

1. Greaves M. Infection, immune responses and the aetiology of childhood leukaemia. Nat Rev Cancer 2006;6:193–203.

Published OnlineFirst September 25, 2015; DOI: 10.1158/2159-8290.CD-15-0892

2. Mullighan CG, Goorha S, Radtke I, Miller CB, Coustan-Smith E, Dalton JD, et al. Genome-wide analysis of genetic alterations in acute lymphoblastic leukaemia. Nature 2007;446:758–64.
3. Mullighan CG, Su X, Zhang J, Radtke I, Phillips LA, Miller CB, et al. Deletion of IKZF1 and prognosis in acute lymphoblastic leukemia. N Eng J Med 2009;360:470–80.
4. Kuiper RP, Schoenmakers EF, van Reijmersdal SV, Hehir-Kwa JY, van Kessel AG, van Leeuwen FN, et al. High-resolution genomic profiling of childhood ALL reveals novel recurrent genetic lesions affecting pathways involved in lymphocyte differentiation and cell cycle progression. Leukemia 2007;21:1258–66.
5. Auer F, Ruschendorf F, Gombert M, Husemann P, Ginzel S, Izraeli S, et al. Inherited susceptibility to pre B-ALL caused by germline transmission of PAX5 c.547G>A. Leukemia 2014;28:1136–8.
6. Shah S, Schrader KA, Waanders E, Timms AE, Vijai J, Miething C, et al. A recurrent germline PAX5 mutation confers susceptibility to pre-B cell acute lymphoblastic leukemia. Nat Genet 2013;45:1226–31.
7. Ward G. The infective theory of acute leukaemia. Br J Child Dis 1917;14:11.
8. Kinlen L. Evidence for an infective cause of childhood leukaemia: comparison of a Scottish new town with nuclear reprocessing sites in Britain. Lancet 1988;2:1323–7.
9. Greaves MF. Speculations on the cause of childhood acute lymphoblastic leukemia. Leukemia 1988;2:120–5.
10. Little J. Epidemiology of childhood cancer. Lyon; 1999 Report No.: 149.
11. McNally RJ, Eden TO. An infectious aetiology for childhood acute leukaemia: a review of the evidence. Br J Haematol 2004;127:243–63.
12. Cobaleda C, Jochum W, Busslinger M. Conversion of mature B cells into T cells by dedifferentiation to uncommitted progenitors. Nature 2007;449:473–7.
13. Nutt SL, Heavey B, Rolink AG, Busslinger M. Commitment to the B-lymphoid lineage depends on the transcription factor Pax5. Nature 1999;401:556–62.
14. Nutt SL, Thevenin C, Busslinger M. Essential functions of Pax-5 (BSAP) in pro-B cell development. Immunobiology 1997;198:227–35.
15. Urbanek P, Wang ZQ, Fetka I, Wagner EF, Busslinger M. Complete block of early B cell differentiation and altered patterning of the posterior midbrain in mice lacking Pax5/BSAP. Cell 1994;79:901–12.
16. Heltemes-Harris LM, Willette MJ, Ramsey LB, Qiu YH, Neeley ES, Zhang N, et al. Ebf1 or Pax5 haploinsufficiency synergizes with STAT5 activation to initiate acute lymphoblastic leukemia. J Exp Med 2011;208:1135–49.
17. Lane AA, Chapuy B, Lin CY, Tivey T, Li H, Townsend EC, et al. Triplication of a 21q22 region contributes to B cell transformation through HMGN1 overexpression and loss of histone H3 Lys27 trimethylation. Nat Genet 2014;46:618–23.
18. Kohlmann A, Schoch C, Schnittger S, Dugas M, Hiddemann W, Kern W, et al. Pediatric acute lymphoblastic leukemia (ALL) gene expression signatures classify an independent cohort of adult ALL patients. Leukemia 2004;18:63–71.
19. Chiaretti S, Li X, Gentleman R, Vitale A, Wang KS, Mandelli F, et al. Gene expression profiles of B-lineage adult acute lymphocytic leukemia reveal genetic patterns that identify lineage derivation and distinct mechanisms of transformation. Clin Cancer Res 2005;11:7209–19.
20. Green MR, Monti S, Dalla-Favera R, Pasqualucci L, Walsh NC, Schmidt-Supprian M, et al. Signatures of murine B-cell development implicate Yy1 as a regulator of the germinal center-specific program. Proc Natl Acad Sci U S A 2011;108:2873–8.
21. Subramanian A, Tamayo P, Mootha VK, Mukherjee S, Ebert BL, Gillette MA, et al. Gene set enrichment analysis: a knowledge-based approach for interpreting genome-wide expression profiles. Proc Natl Acad Sci U S A 2005;102:15545–50.
22. MacKenzie J, Greaves MF, Eden TO, Clayton RA, Perry J, Wilson KS, et al. The putative role of transforming viruses in childhood acute lymphoblastic leukemia. Haematologica 2006;91:240–3.
23. Liu GJ, Cimmino L, Jude JG, Hu Y, Witkowski MT, McKenzie MD, et al. Pax5 loss imposes a reversible differentiation block in B-progenitor acute lymphoblastic leukemia. Genes Dev 2014;28:1337–50.
24. Ford AM, Palmi C, Bueno C, Hong D, Cardus P, Knight D, et al. The TEL-AML1 leukemia fusion gene dysregulates the TGF-beta pathway in early B lineage progenitor cells. J Clin Invest 2009;119:826–36.
25. Tsuzuki S, Seto M, Greaves M, Enver T. Modeling first-hit functions of the t(12;21) TEL-AML1 translocation in mice. Proc Natl Acad Sci U S A 2004;101:8443–8.
26. Futreal PA, Coin L, Marshall M, Down T, Hubbard T, Wooster R, et al. A census of human cancer genes. Nat Rev Cancer 2004;4:177–83.
27. Choi YL, Kaneda R, Wada T, Fujiwara S, Soda M, Watanabe H, et al. Identification of a constitutively active mutant of JAK3 by retroviral expression screening. Leukemia Res 2007;31:203–9.
28. Sato T, Toki T, Kanezaki R, Xu G, Terui K, Kanegane H, et al. Functional analysis of JAK3 mutations in transient myeloproliferative disorder and acute megakaryoblastic leukaemia accompanying Down syndrome. Br J Haematol 2008;141:681–8.
29. Degryse S, de Bock CE, Cox L, Demeyer S, Gielen O, Mentens N, et al. JAK3 mutants transform hematopoietic cells through JAK1 activation, causing T-cell acute lymphoblastic leukemia in a mouse model. Blood 2014;124:3092–100.
30. Papaemmanuil E, Rapado I, Li Y, Potter NE, Wedge DC, Tubio J, et al. RAG-mediated recombination is the predominant driver of oncogenic rearrangement in ETV6-RUNX1 acute lymphoblastic leukemia. Nat Genet 2014;46:116–25.
31. Swaminathan S, Klemm L, Park E, Papaemmanuil E, Ford A, Kweon SM, et al. Mechanisms of clonal evolution in childhood acute lymphoblastic leukemia. Nat Immunol 2015;16:766–74.
32. Swaminathan S, Muschen M. Infectious origins of childhood leukemia. Oncotarget 2015;6:16798–9.
33. Robbiani DF, Deroubaix S, Feldhahn N, Oliveira TY, Callen E, Wang Q, et al. Plasmodium infection promotes genomic instability and AID-dependent B cell lymphoma. Cell 2015;162:727–37.
34. Tsai AG, Lu H, Raghavan SC, Muschen M, Hsieh CL, Lieber MR. Human chromosomal translocations at CpG sites and a theoretical basis for their lineage and stage specificity. Cell 2008;135:1130–42.
35. Crouch S, Lightfoot T, Simpson J, Smith A, Ansell P, Roman E. Infectious illness in children subsequently diagnosed with acute lymphoblastic leukemia: modeling the trends from birth to diagnosis. Am J Epidemiol 2012;176:402–8.
36. Gilman EA, Knox EG. Childhood cancers: space-time distribution in Britain. J Epidemiol Community Health 1995;49:158–63.
37. Cooke J. The incidence of acute leukemia in children. JAMA 1942;119:4.
38. Bolstad BM, Irizarry RA, Astrand M, Speed TP. A comparison of normalization methods for high density oligonucleotide array data based on variance and bias. Bioinformatics 2003;19:185–93.
39. Irizarry RA, Bolstad BM, Collin F, Cope LM, Hobbs B, Speed TP. Summaries of Affymetrix GeneChip probe level data. Nucleic Acids Res 2003;31:e15.
40. Irizarry RA, Hobbs B, Collin F, Beazer-Barclay YD, Antonellis KJ, Scherf U, et al. Exploration, normalization, and summaries of high density oligonucleotide array probe level data. Biostatistics 2003;4:249–64.
41. Tusher VG, Tibshirani R, Chu G. Significance analysis of microarrays applied to the ionizing radiation response. Proc Natl Acad Sci U S A 2001;98:5116–21.
42. Benjamini Yoav, Hochberg Y. Controlling the false discovery rate: a practical and powerful approach to multiple testing. J Roy Stat Soc (Ser B) 1995;57:289–300.
43. Gentleman RC, Carey VJ, Bates DM, Bolstad B, Dettling M, Dudoit S, et al. Bioconductor: open software development for computational biology and bioinformatics. Genome Biol 2004;5:R80.

Published OnlineFirst September 25, 2015; DOI: 10.1158/2159-8290.CD-15-0892

44. Edgar R, Domrachev M, Lash AE. Gene Expression Omnibus: NCBI gene expression and hybridization array data repository. Nucleic Acids Res 2002;30:207–10.
45. Delogu A, Schebesta A, Sun Q, Aschenbrenner K, Perlot T, Busslinger M. Gene repression by Pax5 in B cells is essential for blood cell homeostasis and is reversed in plasma cells. Immunity 2006;24:269–81.
46. Revilla IDR, Bilic I, Vilagos B, Tagoh H, Ebert A, Tamir IM, et al. The B-cell identity factor Pax5 regulates distinct transcriptional programmes in early and late B lymphopoiesis. EMBO J 2012;31:3130–46.
47. Schebesta A, McManus S, Salvagiotto G, Delogu A, Busslinger GA, Busslinger M. Transcription factor Pax5 activates the chromatin of key genes involved in B cell signaling, adhesion, migration, and immune function. Immunity 2007;27:49–63.
48. Cibulskis K, Lawrence MS, Carter SL, Sivachenko A, Jaffe D, Sougnez C, et al. Sensitive detection of somatic point mutations in impure and heterogeneous cancer samples. Nat Biotechnol 2013;31:213–9.
49. Koboldt DC, Zhang Q, Larson DE, Shen D, McLellan MD, Lin L, et al. VarScan 2: somatic mutation and copy number alteration discovery in cancer by exome sequencing. Genome Res 2012;22:568–76.
50. Sanchez-Garcia I, Grutz G. Tumorigenic activity of the BCR-ABL oncogenes is mediated by BCL2. Proc Natl Acad Sci U S A 1995;92:5287–91.

Published OnlineFirst September 25, 2015; DOI: 10.1158/2159-8290.CD-15-0892

AACR American Association for Cancer Research

CANCER DISCOVERY

Infection Exposure Is a Causal Factor in B-cell Precursor Acute Lymphoblastic Leukemia as a Result of *Pax5*-Inherited Susceptibility

Alberto Martín-Lorenzo, Julia Hauer, Carolina Vicente-Dueñas, et al.

Cancer Discov 2015;5:1328-1343. Published OnlineFirst September 25, 2015.